Article Identifier
DOI: 10.22032/dbt.58848
URN: urn:nbn:de:gbv:ilm1-2023isc-021:0

60th ILMENAU SCIENTIFIC COLLOQUIUM
Technische Universität Ilmenau, 4 – 8 September 2023
URN: urn:nbn:de:gbv:ilm1-2023isc:1

TOLERANCING OF CENTERING OF A REFLECTIVE DUAL FIELD-OF-VIEW OPTICAL SYSTEM BASED ON ALVAREZ-PRINCIPLE

Lucas Zettlitzer[(1) (2)], Herbert Gross[(1)], Stefan Risse[(1)], René Theska[(2)]

[(1)] Fraunhofer Institute for Applied Optics and Precision Engineering, 07745 Jena, Germany
[(2)] Technische Universität Ilmenau, 98693 Ilmenau, Germany

ABSTRACT

A new dual state reflective optical relay system based on the Alvarez principle is proposed, which can be used for remote sensing applications. Using the solution found, two different object fields can be imaged using the same optical system. A Three-Mirror-Anastigmat telescope (TMA) is proposed with an intermediate image plane that incorporates a double reflective freeform subsystem as a relay system. By mechanically moving two freeform mirror substrates, this subsystem allows for a discrete change in the total focal length. A deep understanding of the effects of geometric deviations on the system is a crucial prerequisite for ensuring mechanical feasibility and stable optical imaging performance. For this reason, this article focuses on the method and results of tolerancing the subsystem.

Index Terms **–** freeform optics, dual field-of-view, foveated system, tolerancing

1. INTRODUCTION

An overview of the basic methodology for tolerating the centering of a dual-state reflective optical system for space remote sensing is presented in this article. A detailed description of the system concept and optical design process can be found in [1]. The subsequent will provide a brief overview of the system, followed by a description of the methodology and results of a sensitivity analysis.

The basic idea of building the reflective dual field-of-view optical system is to incorporate a mirror relay system into a Three-Mirror-Anastigmat (TMA) as schematically shown in Figure 1. It is intended to switch between the two systems states only within the relay group. The TMA is designed with an intermediate image plane, in which a double reflective freeform subsystem is integrated. The small beam diameter around the intermediate image allows for a compact subsystem design.

The relay group consists of four freeform mirrors and two plane fold mirrors as beam deflectors. The basic concept for the freeform subsystem design is based on the Alvarez principle from 1964 [2]. The original Alvarez concept describes a tandem lens system consisting of two refractive freeform elements shifted perpendicular to the optical axis by an

opposite but equal amount. As a result, a continuous change in focal length can be achieved, which is proportional to the displacements between the lenses and the sag of the surfaces. Unlike classical Alvarez systems, this realization will feature only two discrete configurations rather than a continuous variation in focal length. Furthermore, the arrangement of four movable mirror surfaces enables compensation of axial displacements and thus constant image positioning.

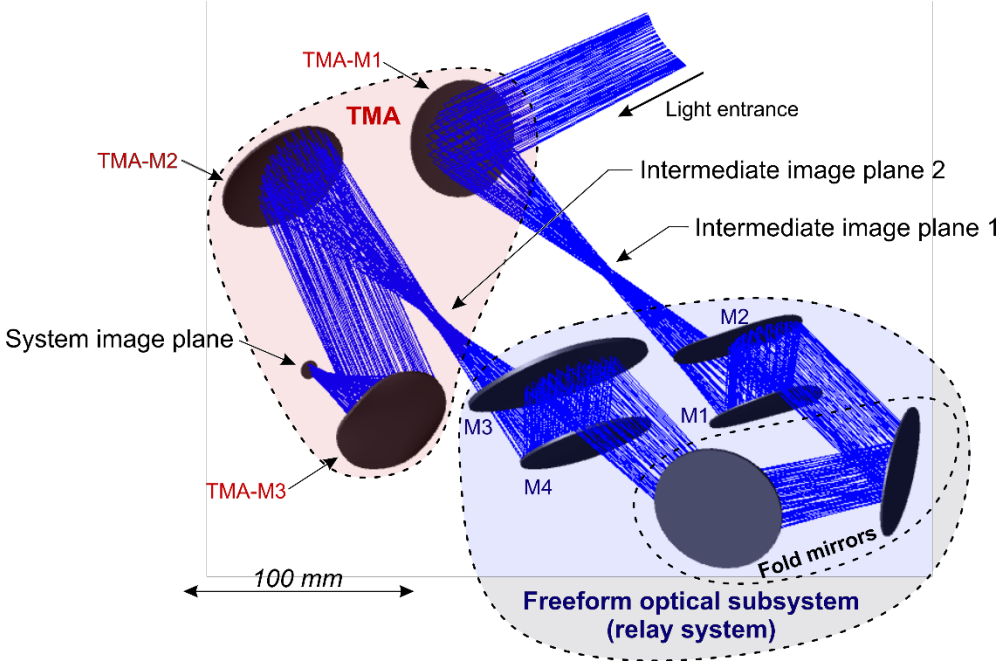

Figure 1: Dual field-of-view reflective optical system

Two freeform surfaces were arranged to form a common mirror substrate (exemplified in Figure 2). A detailed discussion of the application of common mirror substrates can be found in [3]. Especially for freeform surfaces without a common axis of rotation, manufacturing on a common mirror body is preferable. As illustrated in [4], the fabrication of the two freeform surfaces can also be combined with the fabrication of mechanical references on the substrate. Due to machining in one set-up, the relative positions of the mirror surfaces are already fixed. The residual deviations caused by ultra-precision machining are of very small magnitude. A freeform surface usually requires adjustment of all six rigid body degrees of freedom. If two of these mirror surfaces are arranged on a common substrate only six degrees of freedom must be set instead of 12. As a result, the overall assembly of the system is simplified [5, 6].

The resulting two mirror substrates are then displaced in opposite directions by the same amount until they reach their final positions. This movement, in conjunction with a position-constant entrance pupil, illuminates different areas on the mirror surfaces, later referred to as functional areas (Figure 2).

The optical system is optimized for two discrete configurations. In configuration 1, the functional areas -A of M1 to M4 are used, while in configuration 2, the functional areas -B are used. In each of the functional areas, the surface shape varies, resulting in different optical powers per surface area and consequently in two different configurations with different magnifications. When used in conjunction with a telescope, as shown in Figure 1, the two configurations correspond to two different fields of view.

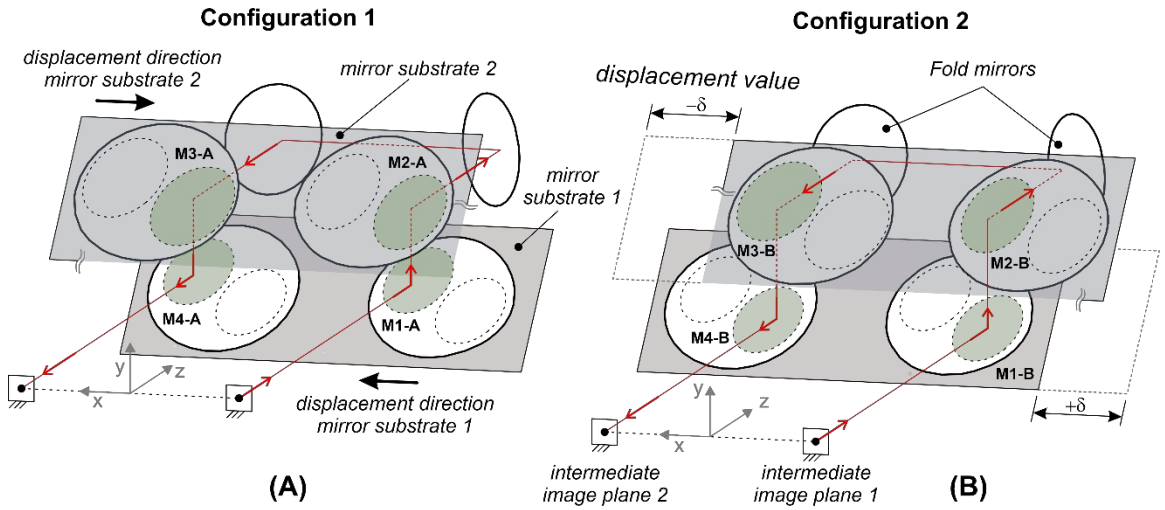

Figure 2: Schematic illustration of the two subsystem configurations. (A) The arrows indicate the direction in which the mirror modules must be displaced in order to reach configuration 2 (B).

2. SUBSYSTEM SPECIFICATIONS

Table 1 summarizes the key specifications of the subsystem. A summary of the most important optical surface parameters can be found in Table 2. The stop is located on the mirror surface M1. The selected variant represents a good balance between the quality of the optical features (related to the subsystem), the integration of the subsystem into the overall system and the mechanical feasibility. Furthermore, it is ensured that the angle of entry into the system can be achieved through the primary TMA mirror. With the given parameters a system performance for configuration 1 of 0,03415 · λ and for configuration 2 of 0,09157 · λ (average of all field points) is achieved.

Table 1: Key system specifications of the subsystem

Parameter	Units	Specification	
		configuration 1	configuration 2
Displacement δ	mm	-11	11
Object distance	mm	100	100
Image distance (Back Focal Length)	mm	100	100
Magnification	-	-1	-0,25
Object numerical aperture	-	0,08	0,02
Image numerical aperture	-	0,08	0,08
Maximum field angle	deg	0,4	1,6
Lateral surface vertices distance (x-distance)	mm	70	
Vertical surface (y-distance)	mm	38	
Wavelength	µm	8	
Ellipticity (all field points averaged)	%	3	15

Table 2: Key specifications of the mirror modules

	Mirror module 1 (M1M4)		Fold mirrors	Mirror module 2 (M2M3)	
	Mirror M1	Mirror M4		Mirror M3	Mirror M2
Surface Type	Zernike-Fringe (max. order: 25)	Zernike-Fringe (max. order: 25)	Flat	Zernike-Fringe (max. order: 25)	Zernike-Fringe (max. order: 25)
Aperture Type	Elliptical x-width: 48 mm y-width: 30 mm	Elliptical x-width: 32 mm y-width: 28 mm	Circular Ø 44 mm	Elliptical x-width: 68 mm y-width: 60 mm	Elliptical x-width: 56 mm y-width: 32 mm
Module size	160 mm x 80 mm (preliminary, not including interfaces)		-	160 mm x 80 mm (preliminary, not including interfaces)	

3. TOLERANCING ASPECTS

In the following figure, an overview is provided to illustrate which tolerances must be considered for the system. Considering that the modules only have to be correctly positioned in relation to each other in two discrete states, it is possible to accomplish this purely through a static analysis of the module positions. This point will be discussed in more detail in the next section.

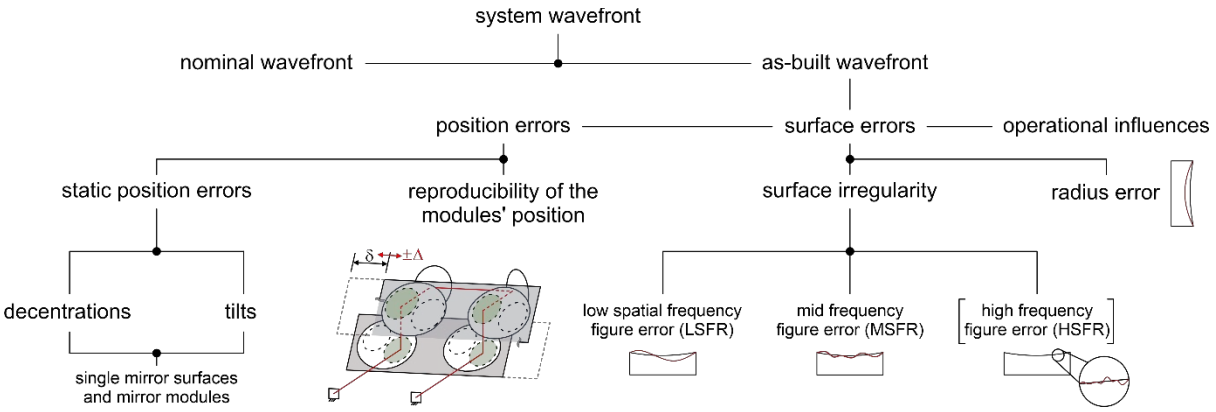

Figure 3: Influences on the system wavefront

Firstly, a general tolerance budget must be determined. The system comprises two configurations: configuration 1, which corresponds to a smaller field of view with higher resolution, and configuration 2, designed for a scene overview application with a larger image field and acceptable lower resolution. Consequently, configuration 1 should only experience a decrease in imaging performance until it reaches the Maréchal criterion ($0{,}0714 \cdot \lambda$). For this purpose, a maximum degradation of up to 35 % with respect to the nominal wavefront error is acceptable.

This article will focus on the freeform subsystem, particularly addressing the tolerances associated with the positioning of the mirror modules. An important aspect of the tolerance analysis is the sensitivity analysis of the mirror module centering. There is still an investigation in progress concerning a tolerancing approach with respect to the expectation of surface form deviations for freeform surfaces with higher surface slopes. Furthermore, the TMA is currently

in the design process. Therefore, corresponding margins are considered for tolerances which are currently not included. A complete tolerance analysis must include all of these points. Accordingly, the following results represent only one aspect of the tolerance analysis and future publications will address the entire tolerancing.

In a first approximation, tolerance margins can be estimated based on the existing subsystem (Table 3). Therefore, it is possible to calculate the maximum allowable degradation of the subsystem (compared to the nominal value) to achieve the required specification in conjunction with the wavefront error of the telescope.

In general, three different models can be used to superimpose wavefront errors. Regardless of whether wavefront errors from individual tolerances or system wavefront errors are to be calculated. The statistical superposition assumes statically independent tolerances. Linear superposition represents the maximum error added by amount, ignoring interdependencies or coupling of tolerances (worst-case scenario). It is possible to use Räntsch's superposition in the case of unknown system behavior and for initial estimations [7]. This is defined as the geometric mean of the results from linear and statistical superpositions.

Assuming an allowable percent degradation for the subsystem (e. g. for configuration 1 +30%), the resultant maximum wavefront error for the telescope can be calculated. The results of all three superposition variants are presented in Table 3.

Table 3: Nominal RMS wavefront and maximal degradation limits per configuration

	referred to	Configuration 1	Configuration 2
Specification	system	0,0714 · λ	0,1237 · λ
Nominal RMS wavefront value	subsystem	0,0342 · λ	0,0916 · λ
Allowed percentage degradation	subsystem	+ 30 % (0,0444 · λ)	+ 20 % (0,1099 · λ)
Resulting maximum wavefront value, based on the allowed percentage degradation of the subsystem	telescope (TMA)	statistical: 0,0560 · λ linear: 0,0270 · λ Räntsch: 0,0388 · λ	statistical: 0,0568 · λ linear: 0,0138 · λ Räntsch: 0,0280 · λ
Margin for surface irregularities of the mirrors	subsystem	10 %	10 %
Allowed relative degradation from position deviations	subsystem	20 %	10 %

Considering linear superposition, only a small wavefront error is permissible for the telescope. In general, the results for statistical and Räntsch superpositions are considered to be feasible. As the subassembly improves, the telescope's tolerance margin increases. The exact breakdown of the percentage deterioration cannot be determined at this time. A detailed analysis of all system components will be possible once the telescope has been designed, the accuracy requirements for it have been determined in more detail, and the manufacturing investigation has been completed.

According to Table 1, the nominal wavefront of the subsystem is 0,0342 · λ for configuration 1 and 0,0916 · λ for configuration 2. Thus, configuration 1 theoretically has a larger tolerance budget than configuration 2. Because all tolerances apply equally to both configurations, configuration 2 represents the more critical design case for defining tolerances.

According to these assumptions, a single position tolerance should result in a degradation of 1 % to 2 % at maximum for configuration 2, and potentially up to 5 % for configuration 1. It is necessary to reach a compromise between the minimum degradation of the system and acceptable tolerances for the subsystem. Further details will be provided about the overall system in the future. The tolerance consideration for the subsystem is critical since it impacts the mechanical design of the mechanism in a significant manner.

3.1 Tolerancing of centering for the subsystem

The initial design of the subsystem in [1] was done with the RMS spot radius as a performance criterion. During the early stages of optimization, RMS spot radius can be considered a robust and consistent parameter, which facilitates a simple and rapid performance evaluation of the system [8]. Following the basic optimization or achieving the basic requirements, the performance criterion can be switched to RMS wavefront error. Moreover, it has some advantages for tolerating as well. The wavefront is therefore capable of providing a holistic assessment of aberrations, and unlike spot radius, it can be measured directly. In turn, this makes it easier to compare real measurement data with theoretical simulations.

The RMS wavefront is calculated as an average of all field points from the merit function in Zemax OpticStudio. When considering the overall system, it is more appropriate to conduct a detailed analysis for all field points. As far as estimating the behavior of the subsystem in general, this procedure is sufficient. The tolerance analysis is performed in the order shown in Table 4 and the corresponding steps are explained subsequently.

Table 4: Tolerance sequence for the subsystem

Nr.	Mirror modules M1M4 & M2M3	Fold mirrors	section
1	Interface error (tilts and z-decenter)	ideal position	3.2.1
2	Clocking error	ideal position	3.2.2
2	Decentration errors	ideal position	3.2.3
3	Monte Carlo simulation	with tilt and distance errors	3.2.4

First, the interface error and the decentrations of the mirror modules were considered separately in order to assess the impact of each on the system's performance. Individual consideration of tolerances does not include compensators. The results were evaluated with the initial tolerance assumptions, followed by a Monte Carlo simulation to assess the overall effect of the tolerances. In addition, this Monte Carlo simulation includes the possibility of folding mirror deviations as well as compensation effects that may occur. The calculations were conducted in Python and the corresponding values were passed to Zemax OpticStudio via its ZOS-API.

3.1.1 Tolerance concept for interface error

A mirror module is typically mounted to a (telescope) housing using three ultraprecise reference planes [4]. As a result of the manufacturing process, there are now deviations between the three reference planes, referred to as interface errors. As a result of this interface error, the mirror module tilts in relation to its nominal position.

The system must be capable of performing adequately in two static configurations. The optical performance that the system takes between these two configurations is not relevant. The

results of this analysis can be used to derive additional conclusions regarding the accuracy required for positioning elements.

The interface error cannot be used as a direct parameter for tolerancing the optical system. It is necessary to convert the height deviation between the interface points into a tilt about the x- and y-axes. To accomplish this, three interface points (Equation 1) are defined in a reference coordinate system (RCS). The coordinate systems and variables which refers to the interface error are illustrated in Figure 4.

$$\begin{matrix} P_1 = (x_1, y_1, z_1) \\ P_2 = (x_2, y_2, z_2) \\ P_3 = (x_3, y_3, z_3) \end{matrix} \rightarrow \begin{matrix} \text{ideal case} \\ z_i = 0 \end{matrix} \quad \begin{matrix} \text{interface error} \\ z_i = \Delta z_{IF,i} \end{matrix} \tag{1}$$

Unless there is an interface error, all three points will be in the same plane $z_1 = z_2 = z_3 = 0$. If there is a difference in z-height (Δz_{IF}) between the interface points, the mirror module tilts. The pivot point's position is determined by the relative difference between the interface points.

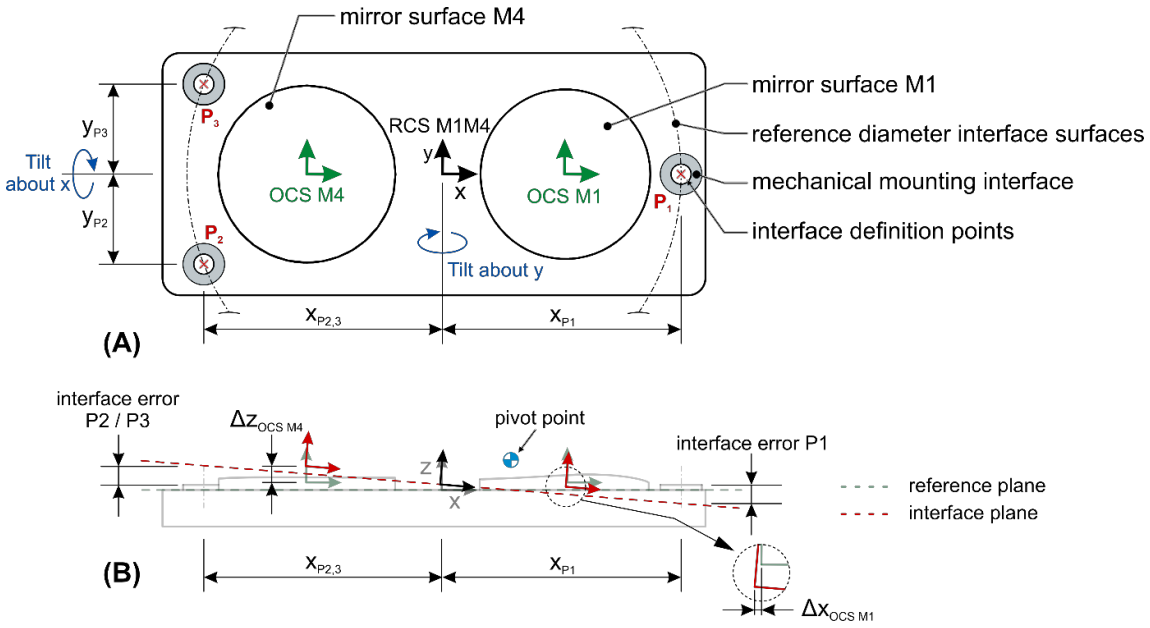

Figure 4: Tolerance concept of interface error (exemplary shown for module M1M4)

The following discussion distinguishes between two types of planes: the reference plane of the module and the realized interface plane. The reference plane represents the plane in the initial (untilted) position of the mirror module. The tolerance plane is the plane formed by the three interface points, each of which has a height error in z. In Figure 5, the basic steps in the calculation are illustrated.

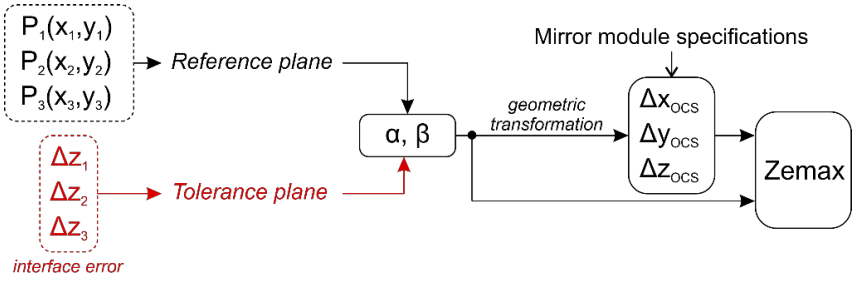

Figure 5: Flowchart illustrating the transfer of the interface errors to Zemax

As a first step, it is necessary to calculate the angles between the two planes. Generally, a plane rotated about x by α, y by β and z by γ will have the following rotation matrix (Equation 2):

$$R = \begin{bmatrix} \cos(\beta)\cdot\cos(\gamma) & -\cos(\beta)\cdot\sin(\gamma) & \sin(\beta) \\ \cos(\gamma)\cdot\sin(\alpha)+\cos(\alpha)\cdot\sin(\gamma) & \cos(\alpha)\cdot\cos(\gamma)-\sin(\alpha)\cdot\sin(\beta)\cdot\sin(\gamma) & -\cos(\beta)\cdot\sin(\alpha) \\ -\cos(\alpha)\cdot\cos(\gamma)\cdot\sin(\beta)+\sin(\alpha)\cdot\sin(\gamma) & \cos(\gamma)\cdot\sin(\alpha)+\cos(\alpha)\cdot\sin(\beta)\cdot\sin(\gamma) & \cos(\alpha)\cdot\cos(\beta) \end{bmatrix} \quad (2)$$

The interface errors will (initially) be in the maximum range of $\pm$ 10 µm and so a small angle approximation can be made. Thus, a first order Taylor expansion can be used to simplify the rotation matrix (Equation 3).

$$R_{Ta} = \begin{bmatrix} 1 & -\gamma & \beta \\ \gamma & 1 & -\alpha \\ -\beta & \alpha & 1 \end{bmatrix} \quad (3)$$

When the simplified rotation matrix is applied to the normal vector of the reference plane, it is possible to calculate the tilt angles. Based on the small angle approximation, the tilt angles of the resulting plane with respect to the x- and y-axes are directly proportional to the x- and y-components of the resulting vector $\vec{r}$ (Equation 4).

$$\overrightarrow{r_{xy}} = R_{Ta}\cdot\vec{n}_{Ref} = \begin{bmatrix} 1 & -\gamma & \beta \\ \gamma & 1 & -\alpha \\ -\beta & \alpha & 1 \end{bmatrix}\cdot\begin{bmatrix} 0 \\ 0 \\ 1 \end{bmatrix} = \begin{bmatrix} \beta \\ -\alpha \\ 1 \end{bmatrix} \quad (4)$$

Thus, it is possible to determine the tilt angles directly from the normal vector of the interface plane. It is important to note that the y-component of this vector $\vec{r}_{xy}$ represents the tilt angle about x and vice versa the x-component represents the tilt angle about y. Aside from the tilting of the mirror modules caused by the interface error, the z-offset (Δz_{OCS}) must also be considered. This corresponds to the distance of the interface plane from the reference plane at x = 0 and y = 0.

After obtaining the tilt angles and z-offset resulting from the interface error, the tilt must be applied to the mirror surfaces. It is therefore necessary to shift the optical coordinate system (OCS) of the respective mirror to the reference pivot with an additional translational transformation. The method also incorporates the calculation of the offsets Δx_{OCS}, Δy_{OCS} and Δz_{OCS} of the optical coordinate systems (see Figure 4-B) that occur during rotation.

3.1.2 Tolerance concept for clocking error

Tolerance analyses for rotation about the z-axis (clocking error) will be performed separately since this is a different error source than the interface error. Nevertheless, the basic principle behind remains the same. The rotation matrix is also defined in this case, but only with a rotation about the z-axis by γ (Equation 5).

$$R_z = \begin{bmatrix} \cos(\gamma) & -\sin(\gamma) & 0 \\ \sin(\gamma) & \cos(\gamma) & 0 \\ 0 & 0 & 1 \end{bmatrix} \quad (5)$$

The clocking error is initially defined in the range of $\pm$ 0,02°, and so a small angle approximation can be made. Thus, a first order Taylor expansion can be used to simplify the rotation matrix (Equation 6).

$$R_{z,TA} = \begin{bmatrix} 1 & -\gamma & 0 \\ \gamma & 1 & 0 \\ 0 & 0 & 1 \end{bmatrix} \tag{6}$$

The center of rotation is also determined by the location of the interface points in x and y, and it is not affected by the height errors of those points. The x- and y-coordinates of the points were determined by an assumption based on the diameters of the mirror surfaces (schematically shown in Figure 4 and 6). It is assumed that the interface points are located as follows:

$$\begin{aligned} P_1 &= (100, -40, 0) \\ P_2 &= (-100, -40, 0) \\ P_3 &= (-100, 40, 0) \end{aligned} \tag{7}$$

Ideally, the mirror module should be designed so that the interface points are located on a common mechanical diameter. This is due to simplified manufacturing procedures [9]. After the mechanical design of the modules, these positions may deviate significantly from these assumptions, making a new analysis necessary. Although the pivot point may vary within a x- and y-deviation of the interface points, this error influence is not considered.

The offset between the center of rotation and the mirror coordinate systems also results in an offset of the optical coordinate systems in the x- and y- directions (Δx_{OCS}, Δy_{OCS}). Since the small angle approximation is used, the offset in the x-direction is negligible. Nevertheless, the y-direction offset is included and the calculation is done as part of the geometric transformation.

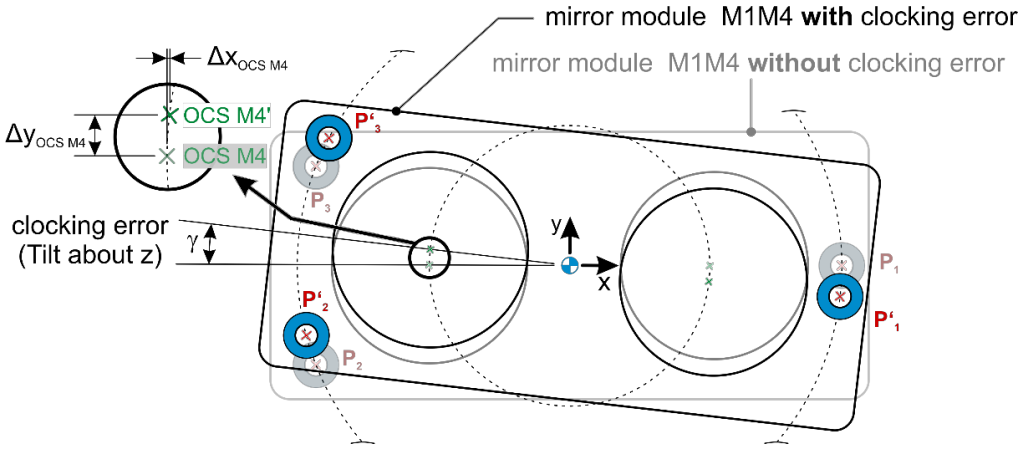

Figure 6: Schematical illustration of the clocking error

3.2 Results of the sensitivity analysis

In the following sections, the change in RMS wavefront is represented as a function of tolerance values. The figures refer to the percentage change in the RMS wavefront with respect to the reference values (Table 1).

3.2.1 Interface error

For the analysis of the interface error, random, but normally distributed, z-deviations ($\Delta z_{IF,i}$) were generated in the range of -10 µm to 10 µm. The results in Figure 7 are related to the mirror module M1M4, and the results in Figure 8 are for the mirror module M2M3. The axes of the diagrams depict the tilt about x and tilt about y caused by the interface error. The green

gradations indicate the maximum tilt angles associated with interface errors of ±2 µm, ±5 µm and ±10 µm. When the module is tilted around the x-axis, the interface error is less significant than when it is rotated around the y axis, due to the larger levers. Data points are colored according to the percentage change of the RMS wavefront indicated in the legend of the figures.

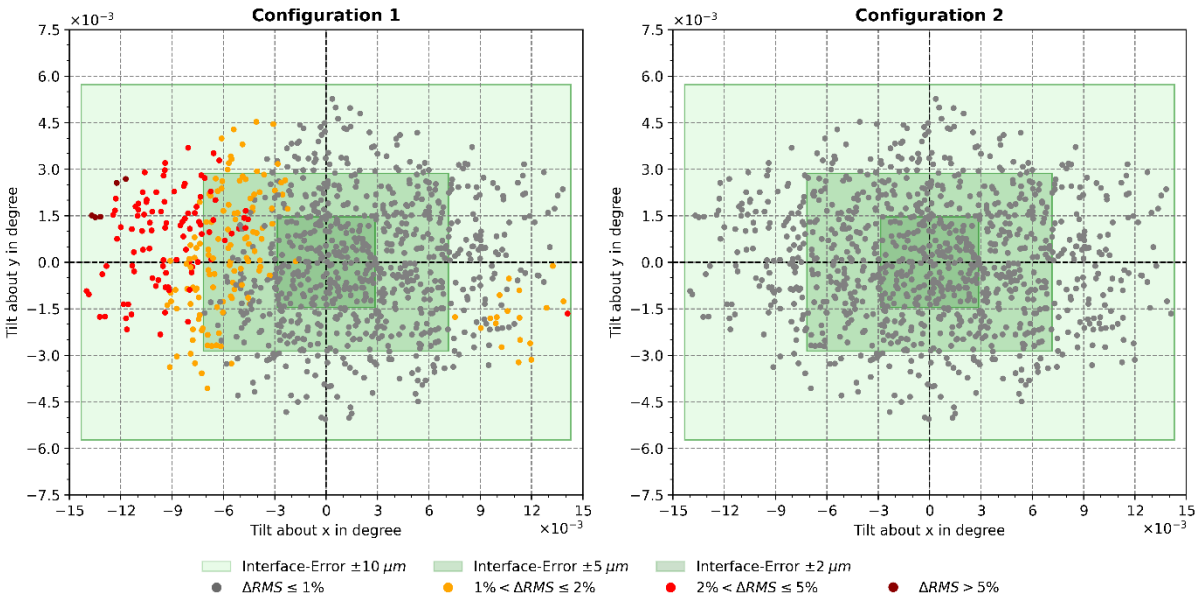

Figure 7: Impact of interface error on RMS wavefront of mirror module M1M4

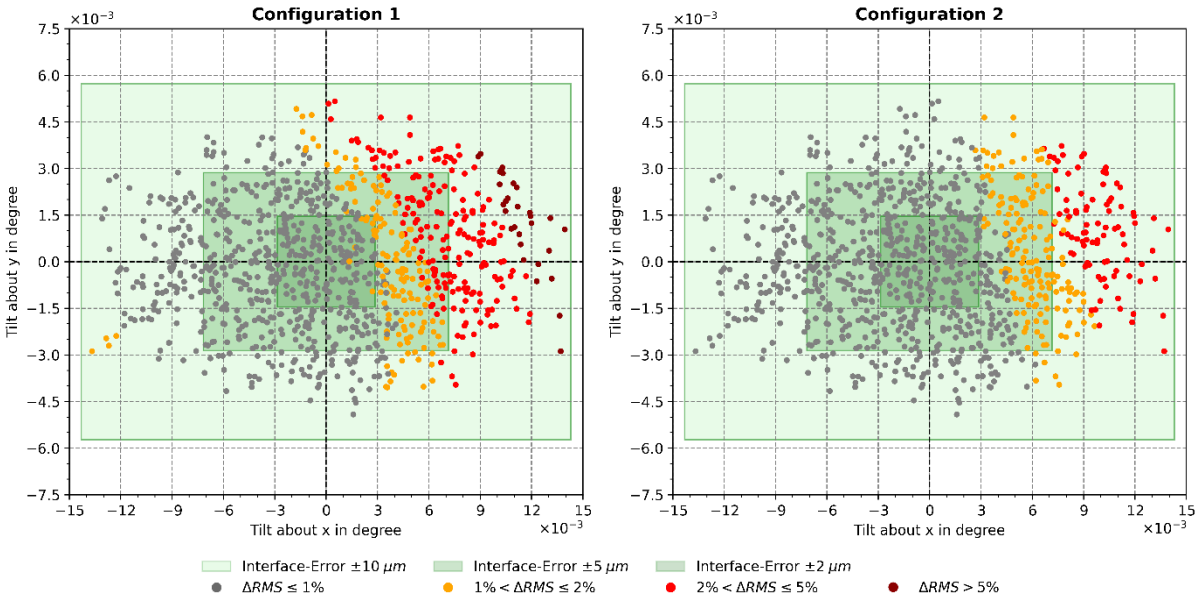

Figure 8: Impact of interface error on RMS wavefront of mirror module M2M3

An interface error has a more significant effect on the M2M3 module than it does on the M1M4 module. This can be seen by the fact that more systems regarding M2M3 experience a change of over two percent than M1M4 (for both configurations). Also, tilt angles that are already small (points near the origin) contribute to larger changes. As regards the same module, configuration 1 is more critically affected by the interface error than configuration 2.

An interface error of ±10 µm for Configuration 1 for module M2M3 is considered critical. Although some systems have a RMS change greater than 5 %, these are mainly in the marginal range and are likely to be counterbalanced by later occurring compensation effects in the system. During the Monte Carlo simulation, a maximum interface error of ±10 µm is assumed.

3.2.2 Clocking error

Figure 9 illustrates the percentage change in the RMS wavefront for both configurations as a function of the corresponding clocking error. This analysis was conducted with 1000 systems uniformly distributed over the tolerance interval (± 0,02°). A polynomial is used to fit the results.

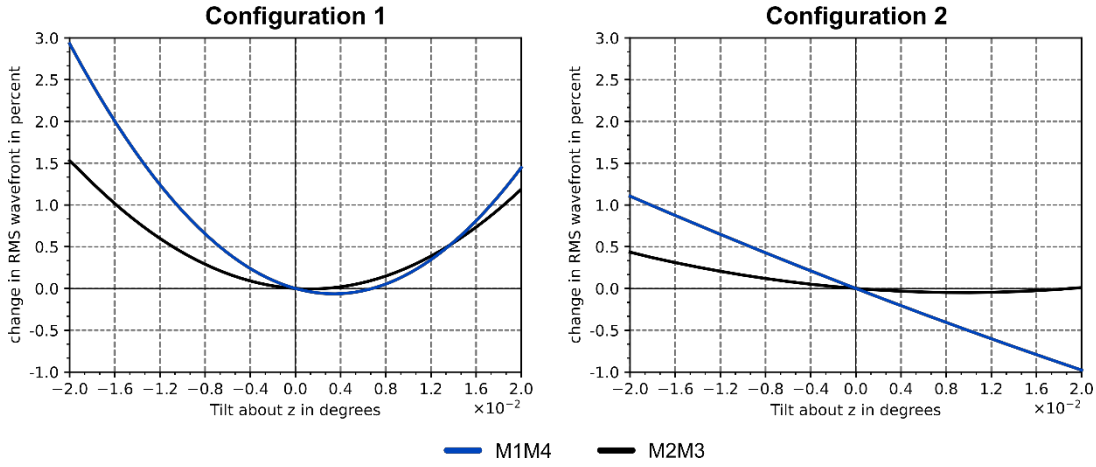

Figure 9: Impact of clocking error on RMS wavefront of mirror module M1M4 and M2M3

Configuration 1 is more sensitive to clocking errors than configuration 2. Furthermore, the mirror module M1M4 is more sensitive. The system's degradation at the outer tolerance limits is slightly outside the acceptable range, but it can still be classified as acceptable.

3.2.3 Decentration error of the mirror modules

This section addresses the decentering error in relation to the final position of the mirror modules. Figures 10 and 11 illustrate the impact of axially and laterally (related to the local coordinate system) decentered mirror modules on system performance. In both directions, the initial tolerance assumption is ±10 µm. A total of 1000 systems were analyzed with equal distributions of tolerances for each. The contour lines are also shown in the figures in order to provide a better understanding of the RMS change.

In Figure 12, the results of a pure parallel z-deviation are shown. Again, a total of 1000 systems are uniformly distributed across the tolerance interval (± 40 µm) and a polynomial is used to fit the results.

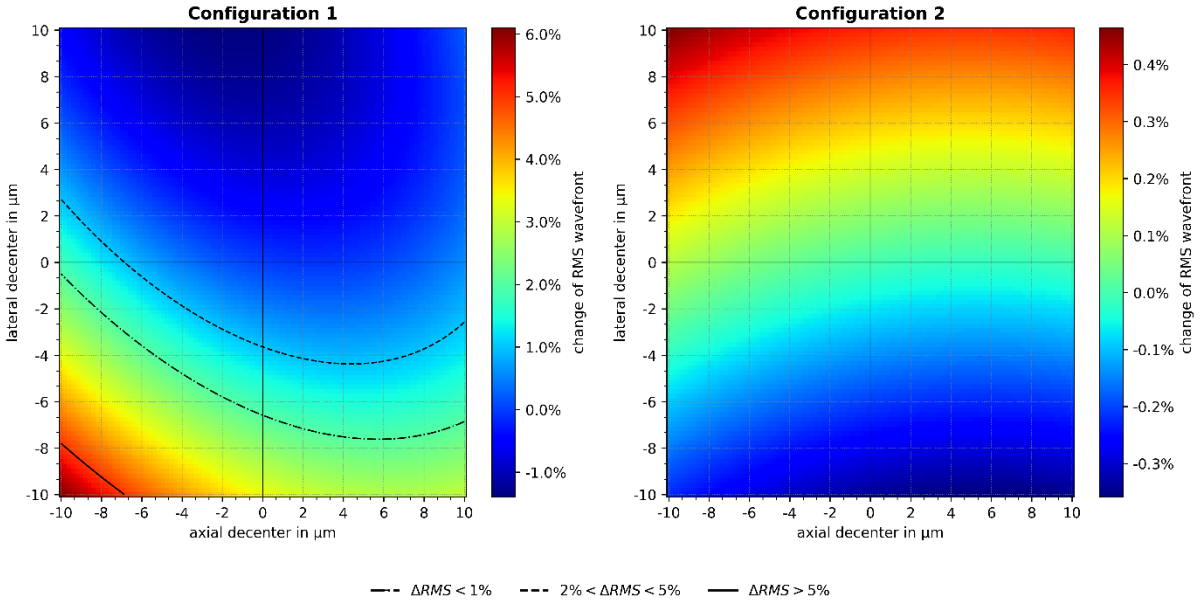

Figure 10: Impact of decentrations errors of mirror module M1M4

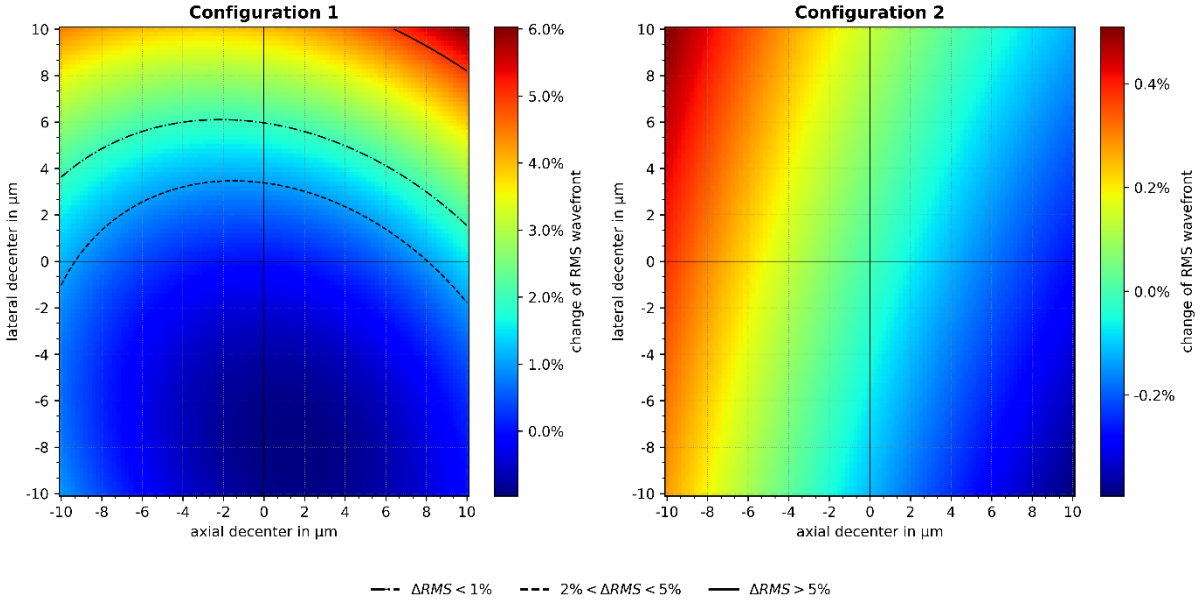

Figure 11: Impact of decentrations errors of mirror module M2M3

There are similar effects on the wavefront error caused by the decentrations of the two mirror modules in this case. The error pattern for configuration 1 is quasi-symmetrical around the x-axis for both modules. The maximum percentage change of configuration 1 is exceeded only when both axial and lateral deviations are near the tolerance limits. Thus, the decentering tolerance is reduced to ±8 µm.

Similar conclusions can be drawn regarding the error influence of module distance in the z-direction (Figure 12).

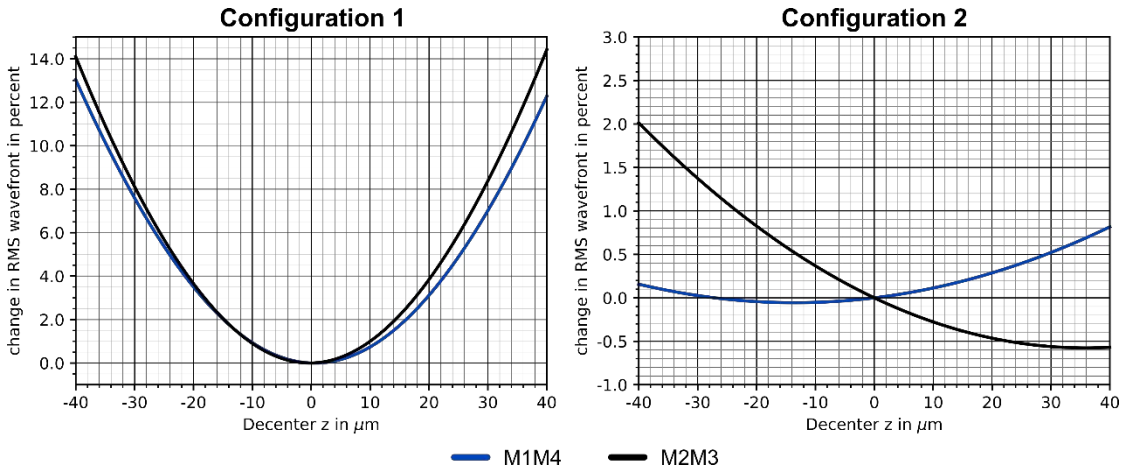

Figure 12: Impact of distance error (z) on RMS wavefront of mirror module M1M4 and M2M3

Configuration 1 is significantly more sensitive than configuration 2. According to the initial tolerance assumptions for configuration 1, the occurring percentage change is significantly greater than the maximum allowed percentage change. It is therefore necessary to reduce the tolerance limit for module distance to ± 30 µm.

3.2.4 Monte Carlo simulation

The Monte Carlo simulation is used to estimate the performance of the total system under the influence of all tolerance influences. The stochastic Monte Carlo simulation assumes that tolerances are superimposed according to a pure normal distribution and that causes are independent. Currently, no compensators are being considered that interfere with the statistics. Consequently, the results can serve as a system indicator and be viewed as superimposed sensitivities, but not as complete subsystem tolerancing. This consideration is done in the context of the overall system, as conceptually shown in Figure 1.

The overall simulation includes the position errors of folding mirrors as well as individual position deviations of the mirror surfaces on the mirror module. The latter are determined by the accuracy of the diamond processing and cannot be altered. The values are derived from measurements made at Fraunhofer IOF of previous systems.

Table 5: Tolerance assumptions for Monte Carlo simulation. Coordinate data are given in the local coordinate system of the mirrors.

Mirror	Error source	Tolerance values	Resulting errors
Mirror modules M1M4 & M2M3	interface error	± 10 µm	tilt about x/y, decenter z
	decentration errors	± 8 µm	decenter x/y
	distance error	± 30 µm	decenter z (distance deviation)
	clocking error	± 0,02 °	decenter x/y, tilt about z
	decentration errors of individual mirror surfaces	± 4 µm	decenter x/y
	tilt error of individual mirror surfaces	± 0,0015 °	tilt about x/y
Fold mirrors	(individual) distance error	± 50 µm	decenter z (distance deviation)
	tilt error	± 0,01 °	tilt about x/y

During the Monte Carlo simulation, different effects from different error sources overlap. Table 5 shows the types of errors, their tolerance assumptions, and their effects on the system. All tolerance values are assumed to have a normal distribution with an expected value of μ = 0 and a standard deviation of $\sigma = ⅓ \cdot \mu$. The simulation considers a total of 1000 systems.

The folding mirrors were considered independently of each other. Because folding mirrors are plane surfaces and deviations of the surfaces are not considered, local decentrations in the x and y directions have no effect on the performance of the system. In Figure 13, the result of the Monte Carlo simulation is summarized in the form of a histogram.

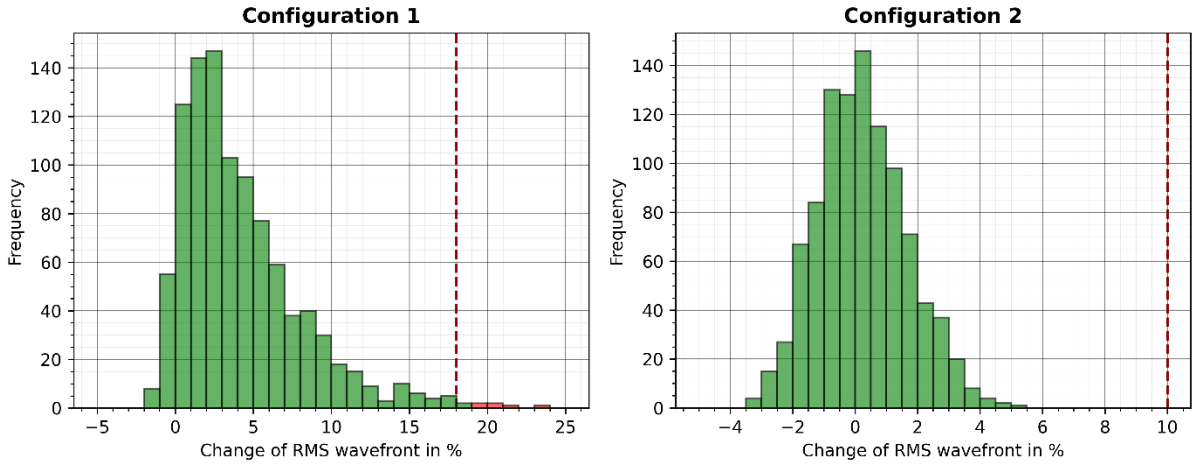

Figure 13: Monte Carlo simulation histogram for the subsystem. The red lines indicate the maximum permissible system degradation caused by position tolerances.

In configuration 2, all systems are within the maximum allowable degradation range. Considering configuration 1, seven systems are not in compliance with the specifications as indicated in Table 3. Each of the seven systems represents a different combination of maximum tolerance limits. In this regard, it is assessed as not critical in the first instance and the subsystem can be expected to meet the requirements assuming realistic position tolerances.

4. CONCLUSION

For a dual-state optical system, which can switch between two discrete fields with the help of a freeform optical subassembly, the methodology for the position tolerancing of the mirror modules has been presented. There was an alternative method presented for evaluating the effects of tilting the mirror modules. Instead of specifying tilt angles directly, the interface error between mirror modules and the housing structure has been used. It is still possible to draw conclusions about the accuracy of the alignment between the two modules despite the fact that it is a dynamic system. Through this analysis, a solid basis has been laid for the mechanical implementation of the subsystem, since concrete requirements for accuracy have now been established. A complete tolerance analysis and re-adjustment of the centering tolerances must be done once the results of the ongoing manufacturing tests for the freeform surfaces are available and the TMA design has been finished. However, the basic methodology and magnitude of tolerances are unlikely to require significant change.

REFERENCES

[1] L. Zettlitzer, H. Gross, S. Risse, and R. Theska *et al.,* "Reflective dual field-of-view optical system based on Alvarez-Principle." [Manuscript submitted for publication], 2023.

[2] L. W. Alvarez, "Two-Element variable-power spherical lens," United States Patent and Trademark Office, *US3305294A,* 1964.

[3] S. Scheiding, S. Risse, A. Gebhardt, C. Damm, T. Peschel, and R. Steinkopf *et al., "*Verfahren zur Fertigung einer optischen Anordnung mit mindestens zwei optischen Funktionsflächen, optisches Gerät und Vorrichtung zur Durchführung des Verfahrens," German Patent and Trade Mark Office, *DE102009041501,* 2009.

[4] M. Beier *et al.,* "Development, fabrication, and testing of an anamorphic imaging snap-together freeform telescope," *Appl. Opt.*, vol. 54, no. 12, p. 3530, 2015.

[5] S. Scheiding, "Vereinfachung der Systemmontage von metalloptischen IR-Spiegelteleskopen," Dissertation, Fakultät V - Verkehrs- und Maschinensysteme, Technische Universität Berlin, Berlin, 2014.

[6] M. Beier, "Fertigung und Kompensation von metalloptischen Hochleistungsspiegelsystemen für den visuellen Spektralbereich," Dissertation, Physikalisch-Astronomischen Fakultät, Friedrich-Schiller-Universität Jena, Jena, 2017.

[7] H. Gross, H. Zügge, and M. Peschka, Eds., "Aberration Theory and Correction of Optical Systems," (Handbook of optical systems / ed. by Herbert Gross Vol. 3), Wiley-VCH, Weinheim, 2007.

[8] W. J. Smith, "Optical engineering: The design of optical systems," 4th ed., McGraw-Hill. New York: McGraw-Hill, 2008.

[9] L. Zettlitzer *et al.,* "Design and fabrication of a miniaturized metallic telescope for earth observation," in 4S-Symposium 2022 Proceedings, Vilamoura, 2022.

CONTACTS

Lucas Zettlitzer — email: lucas.zettlitzer@iof.fraunhofer.de; ORCID: https://orcid.org/0000-0001-5515-2931

Univ.-Prof. Dr. René Theska — email: rene.theska@tu-ilmenau.de

